Appl. Phys. B 55, 463–477 (1992)

Applied Physics B Photophysics and Laser Chemistry

Intra-Cavity Spectroscopy with Diode Lasers

V. M. Baev, J. Eschner, E. Paeth, R. Schüler, and P. E. Toschek

Institut für Laser-Physik, Universität Hamburg, W-2000 Hamburg 36, Fed. Rep. Germany

Received 2 June 1992/Accepted 24 August 1992

Abstract. A multi-mode diode laser with an external cavity is studied experimentally and theoretically for its application to intra-cavity spectroscopy. One facet of a typical $Ga_{0.89}Al_{0.11}As$ laser diode was antireflection-coated by deposition of HfO_2 such that 10^{-3} residual reflectivity was left over. This diode was placed in an external optical cavity. The emission spectrum of this diode laser is highly sensitive to any frequency-dependent loss in the cavity, and the detectivity of such a loss grows with the pump rate. Even close to threshold, the absorption at 780 nm of Rb atoms with a density of $5 \times 10^{10}\,cm^{-3}$ has been detected. An adequate model for diode lasers based on rate equations and including frequency-dependent gain saturation is developed and applied to the calculations of output spectra. The sensitivity of these spectra to intra-cavity absorption is determined by the overall cavity loss – which is rather high – and the fraction of spontaneous emission in the total emission, in contrast with dye lasers where it is limited by nonlinear mode coupling. Various criteria for the sensitivity are suggested. The smallest detectable absorption with a perfectly antireflection-coated laser is $10^{-6}\,cm^{-1}$. Improvement of the characteristics of the laser diode would increase the sensitivity.

PACS: 42.55.Bi, 42.55.Px, 42.65.Ft

Intra-cavity laser spectroscopy (ICLS) is a powerful spectroscopic technique of extreme sensitivity [1–3]. Although successfully used for a long time, its practical application is still limited due to the lack of appropriate broadband lasers. Dye or colour-centre lasers, which are mostly used for measurements of intra-cavity absorption (ICA), require another laser for being pumped, e.g. a costly argon-ion laser. That makes the present equipment for intra-cavity measurements rather expensive and bulky. Furthermore, these lasers operate mostly in the visible and near-IR range, where molecules not usually have strong absorption. From these points of view diode lasers have significant advantages, and they might be good candidates for a commercial intra-cavity spectrometer.

In this paper we present an experimental and theoretical study of potential features of an intra-cavity diode-laser spectrometer. The investigations involve a typical GaAlAs laser diode. In Sect. 1 we describe the extension of this laser by an external cavity and technical problems associated with the AR coating of the diode laser facets. Experimental spectra obtained with a broadband diode laser are presented in Sect. 2. A detailed model of the broadband diode laser is introduced in Sect. 3. This model is based on rate equations and takes into account specific features of diode lasers. Parameters of the model have been estimated from various experimental data and agree with elsewhere-reported properties of diode lasers. The solutions of the rate equations, presented in Sect. 4, are in a good agreement with the observed spectra. In Sect. 5 we determine criteria for the sensitivity of an intra-cavity diode-laser spectrometer and estimate its sensitivity limits in comparison with existing intra-cavity spectrometers operating on the basis of a dye laser. The main results are summarized in Sect. 6.

1 Preparation of the Diode Laser

The gain of diode lasers is usually so large that they operate without any external resonator mirrors but just on the feedback that is supplied by the light reflected from the cleaved diode facets. In GaAlAs this reflection amounts to as much as 32% due to the high refractive index of semiconductors [Fig. 1(a)]. However, for measurements of ICA a sample should be inserted into the laser cavity. An extra resonator that is to house an absorptive medium and that is composed of one of the diode facets and a third mirror might be optically coupled to the laser diode. Such an arrangement represents an inhomogeneously filled three-mirror oscillator, not well-suited for sensitive measurement of absorption. For this purpose, the reflection from at least one of the laser facets has to be suppressed and substituted by feedback from an external cavity mirror. This suppression can be achieved, e.g., by depositing an antireflection (AR) coating onto the laser facets [4], or by special preparation

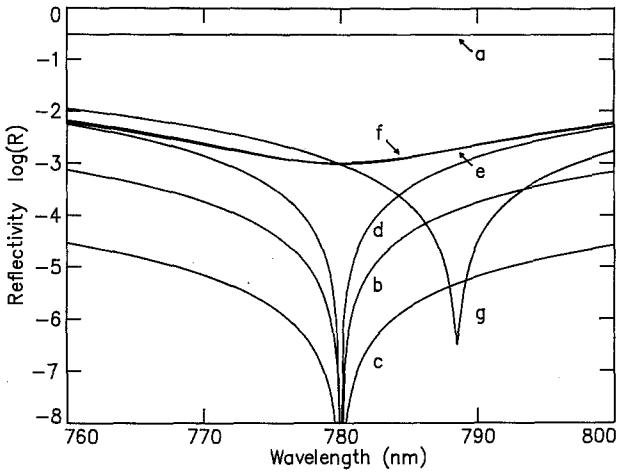

Fig. 1. Spectrum of reflectivity: Uncoated GaAlAs laser facet *(a)*, facet with optimized single *(b)* and double *(c)* AR coating, with single AR coating over protection film *(d)*, and the facet with a single AR coating over the protection film which is 28% thinner *(e)*, with a single AR coating having 3.3% smaller refractive index *(f)* and 3% larger thickness *(g)*

of the diode with the waveguide tilted with respect to the cleaved facets [5].

In our experiment we have used Hitachi HL7801 cw $Ga_{1-x}Al_xAs$ double heterojunction index-guided injection lasers with a channeled substrate planar (CSP) structure [6]. This type of lasers is manufactured in large quantities; therefore the technology of its production is well optimized, and it is inexpensive. It operates at room temperature in the spectral range of 780 nm with a threshold current of about 50 mA. We have chosen these lasers because of their low optical loss and high reliability. The diodes have been dismantled from the original housing and mounted onto copper plates designed for insertion into an evaporation chamber or into a laser cavity; they provide the possibility of temperature control for the diode.

The active layer of the laser is 0.1 μm thick p-type $Ga_{1-x}Al_xAs$, sandwiched between p-type and n-type $Ga_{1-y}Al_yAs$. The width of the active region is about 3 μm [6]. The concentration x of Al in the active layer determines the wavelength of the laser operation. In our laser $x = 0.11$ and the wavelength of operation is $\lambda = 780$ nm (Eq. 1.4 in [7]). The corresponding refractive index n_a of the nonexcited active layer at the wavelength of laser emission is 3.63 [8]. Correction for the presence of injected carriers in the operating laser diode [9] reduces this value to 3.62. The concentration y of Al in the cladding materials is 20–25% greater than x for efficient confinement of the laser light [6]. With $y = 34\%$, the refractive index n_c of the cladding material at the laser wavelength is 3.44 [8].

Antireflection coating of the active material can be accomplished by deposition of a film having the thickness h_1 and the refractive index n_1. These parameters, calculated for normal incidence of plane optical waves onto a large surface, are given by Fresnel's formulas as

$$n_1 = \sqrt{n_a n_0}\,, \tag{1}$$

$$h_1 = m\lambda/4n_1\,, \qquad m = 1, 3, 5, \ldots\,, \tag{2}$$

where n_0 is the refractive index of the ambient medium, air. AR coating of our laser would require the deposition of a film with the refractive index $n_1 = 1.903$ and the thickness $h_1 = 0.1025$. However, the optimum film parameters deviate from these values due to the large divergence of the laser beam. In our laser the beam divergence (FWHM) parallel to the junction is 15° and perpendicular to the junction 30° [6]. Based on these data we have numerically calculated the optimum parameters of AR coating for our laser using a theory developed for two-dimensional waveguide devices, which takes into account the step of the refractive index from the active zone to the cladding [10]. We have also proved that the better three-dimensional model provides only a negligible correction. The calculated film parameters $n_{1,\mathrm{opt}} = 1.858$ and $h_{1,\mathrm{opt}} = 0.258\lambda/n_{1,\mathrm{opt}} = 0.1804\,\mu\mathrm{m}$ warrant the residual power reflectivity to become less than 10^{-8} at $\lambda = 780$ nm. The spectral reflectivity of a facet coated with these parameters is shown in Fig. 1(b). The spectral width of the reflectivity at $R \leq 10^{-3}$ is 47.1 nm, and at $R \leq 10^{-4}$ it is 14.8 nm.

A much broader spectral width of the AR band can be obtained by deposition of a double-layer AR coating [11]. An example of the reflectivity of this coating, calculated for $n_1 = 2.71$, $h_1 = 0.0731\,\mu\mathrm{m}$ and $n_2 = 1.46$ (SiO_2), $h_2 = 0.139\,\mu\mathrm{m}$, is shown in Fig. 1(c). The double-layer AR coating results in the residual reflectivity being some ten times smaller than the single-layer coating.

All commerical diode lasers are coated with a protective film of Al_2O_3 or SiO, characterised by its thickness h_p and refractive index n_0. For undiminished reflectivity, this film should have the thickness $h_p = \lambda/2n_p$ (more precisely, for the divergent beam $h_p = 0.51\,\lambda/n_p$). Unfortunately, even at its optimum thickness the film shifts the optimum coating parameters and the resulting spectrum of reflection. The protective film of our laser is made of SiO with $n_p = 2.00$. The optimum parameters of the AR coating are then $n_1 = 1.89$ and $h_1 = 0.1046\,\mu\mathrm{m}$. From the calculated reflection spectrum [Fig. 1(d)] we see that the presence of the protective film results in ten times higher residual reflectivity and in reduced spectral width (17.4 nm on the level 10^{-3}, and 5.4 nm on the level 10^{-4}).

We have observed, however, that h_p deviates up to 30% from its optimum value. In principle this deviation can be compensated for by appropriate alteration of the thickness h_1 and refractive index n_1 of the AR coating. For that purpose h_p would have to be known. In practice, however, one estimates h_p only in the course of the coating process and compensates for its deviation only partially by optimising h_1, whereas n_1 is kept adjusted such as to correspond to the optimum value of $h_p = 0.51\,\lambda/n_p$. Therefore, the achievable minimum reflectivity is increased. Deviation of h_p by 28% from its optimum value results in 10^{-3} residual reflectivity [Fig. 1(e)]. Less than 10^{-4} reflectivity can be achieved if the deviation of h_p does not exceed 15%.

Several substances with adequate index of refraction could be used for AR coating of GaAlAs lasers: Si_3N_4, SiO, GeO_2, Y_2O_3. Here, HfO_2 was used; it was evaporated by an electron beam in the presence of oxygen at controlled

pressure inside an evaporation plant (BAK 600, Balzers AG). When adjusting the pressure in the range (0.5–4) $\times$ 10^{-4} mbar, we control the refractive index of the film in the range 1.82–1.96 with 0.02 inaccuracy. The residual reflectivity $R_{\min}$ determined by this inaccuracy is less than 10^{-4}. Deviation of the refractive index by 0.06 would increase $R_{\min}$ to 10^{-3}, as shown in Fig. 1(f).

The rate of HfO_2 deposition was 0.37 nm/s, and the duration of the coating process varied between 200 and 400 s, depending on the thickness of the protective film. During the deposition the film thickness was controlled by measuring the light emitted from the opposite facet of the laser [12]. In order to allow for heat relaxation of the HfO_2 source, the deposition was terminated by switching off the electron beam 2–3 s before the emission reached its minimum. A 3 s error of the switching causes 1 nm uncertainty of the film thickness; it still provides for $R \leq 10^{-4}$ at 780 nm. Figure 1(g) shows a calculated reflection spectrum, when the deposition time of HfO_2 is extended 8.7 s over its optimum duration. In this case, the wavelength of $R_{\min}$ is shifted to 789 nm, and the reflectivity at 780 nm is 10^{-3}. The deposited film of HfO_2 is chemically stable and its exposure to the air does not significantly change its properties.

The reflectivity of the coated facet has been measured by spectral modulation of the diode emission at the original threshold current [13]. This value is determined more precisely from the emission spectrum of the coated crystal in an external cavity, as described in Sect. 4.

The lowest reflectivity achieved so far in our experiments was about 10^{-3}. It is limited by deviations of the experimental parameters mentioned above from their optimum values, in particular of the thickness h_p of the protective film. Even this incomplete elimination of the reflectivity allows the construction of a workable diode laser with an external cavity.

2 Experiment

The experimental setup is shown in Fig. 2. The diode laser is mounted on a copper plate whose temperature is controlled by Peltier elements. The pump current is provided by a car battery. The laser cavity is formed by an external Al-coated mirror M1, aligned by piezo translators, and by the uncoated facet of the diode M2 with reflectivity $R_2 = 32\%$. The length of the cavity is 72 cm. Two three-component lenses (Rodenstock, numerical aperture 0.45), mounted on $X - Y - Z$ translation stages, are used for collimating the diode laser emission. One lens, placed inside the cavity, focuses the emission that emerges from the AR coated facet onto the mirror M1 and the reflected light back into the diode. The laser cavity also includes an ICA cell, which is a heat pipe oven filled with Rb, and an acousto-optical deflector AOD1 (ISOMET IMD 80 H 776, 100 ns rise time) used for switching off the laser emission in measurements of the spectral dynamics. Another acousto-optical deflector AOD2 used for time-resolved measurements is placed between the laser and the spectrograph. The laser spectrum is detected by a 1 m Czerny-Turner spectrograph (Jarrel-Ash, 0.2 cm^{-1} spectral

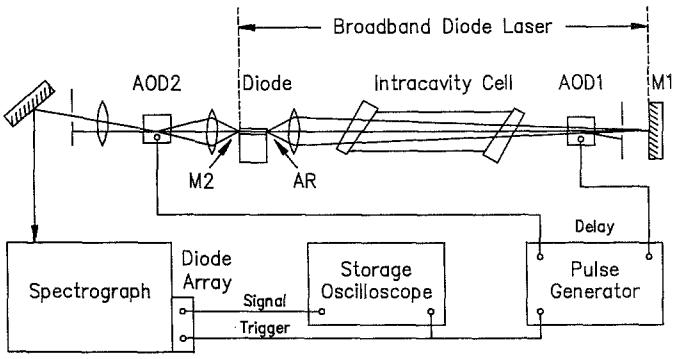

Fig. 2. Experimental setup. AOD1 and AOD2 are acousto-optical deflectors; M1 and M2 are resonator mirrors; AR is the antireflection coating

resolution) with a 1728-channel diode array (Thomson CSF, model TH 7801) and recorded with a digital storage oscilloscope (Scientific Instr., model SMRII, 64 k channels, 12 bit resolution). The modes of the external cavity with 210 MHz spacing are not resolved, only their envelope can be seen in the spectra.

The threshold of the diode laser with external cavity almost equals the threshold of the original laser before coating. Therefore, we estimate the efficiency R_1 for coupling laser light by the external mirror back into the crystal to be about the same as the reflection from the uncoated facet, 32%. The coupling efficiency is limited by the numerical aperture of the lens, its spherical aberrations, the astigmatism of the laser light, and by the loss in the external cavity.

ICA measurements have been carried out with rubidium vapour in the cell. The maximum of the diode laser emission was temperature-tuned to the Rb resonant transition $5S_{1/2} \Leftrightarrow 5P_{3/2}$ at the wavelength 780.027 nm. The density N_{Rb} of the rubidium vapour was set to values ranging from 1×10^6 to 3×10^{11} cm^{-3} by setting the cell temperature between 240 K and 373 K. There is 1 bar argon in the cell and the Rb absorption line is purely collision-broadened with 26 GHz spectral width (FWHM) [14], which is spectrally resolved.

Characteristics of output vs current of the diode laser with external cavity are shown in Fig. 3. Curve *a* shows the output power vs the pump current J, curves *b* and *c* show it with additional broad-band loss in the cavity. This loss is due to calibrated neutral density glass filters of 52% and 34% transmission, respectively.

Stationary emission spectra of the diode laser with intracavity Rb absorption have been recorded at various Rb concentrations and pump levels. Series of these spectra at constant absorption and at constant pump current are shown in Figs. 4, 5. In Fig. 4, $N_{Rb} = 5 \times 10^{10}$ cm^{-3} ($T = 323$ K) with the pump current varied below and above the laser threshold ($J_{th} \cong 46$ mA). Conspicuous features of the spectra are: *(i)* the condensation of the laser output close to the gain maximum; *(ii)* the etalon structure corresponding to the length of the diode crystal, which is the result of imperfect AR coating of the facet, and *(iii)* the Rb intracavity absorption at the centre of the emission profile. All these phenomena become more pronounced upon increasing the pump current. The linewidth of the ICA is some five times smaller than the free spectral range of the etalon

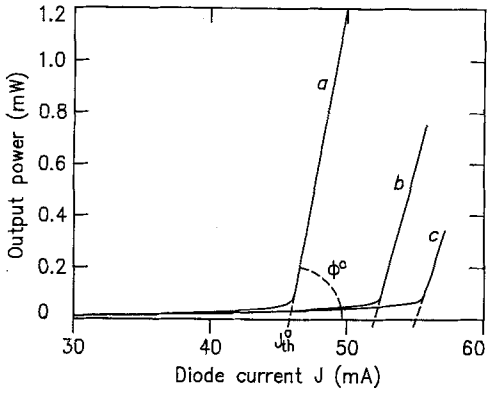

Fig. 3. The output power of the diode laser with extended cavity vs pump current J at broad-band cavity extra loss $\gamma_f = \gamma - \gamma_0 =: 0$ *(a)*, $2.7 \times 10^8\,s^{-1}$ *(b)*, and $4.5 \times 10^8\,s^{-1}$ *(c)*. J_{th}^0 is the threshold current, and $S^0 = \mathrm{tg}\,\Phi_0$ is the slope efficiency at $\gamma_f = 0$

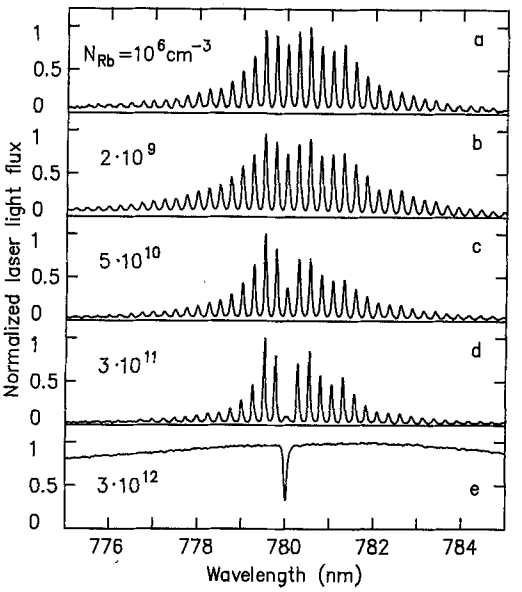

Fig. 5. Normalized output spectra of the diode laser with extended cavity at various densities N_{Rb} in the cavity, and at the pump rate of 46 mA *(a–d)*; the absorption spectrum of Rb vapour outside the laser cavity at the density $N = 3 \times 10^{12}\,cm^{-3}$ *(e)*

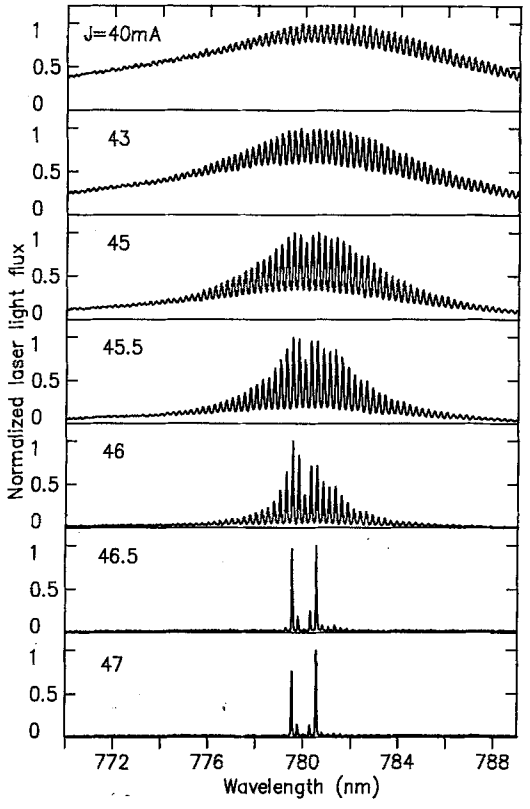

Fig. 4. Normalized output spectra of the diode laser with extended cavity showing ICA of Rb at the density $N_{Rb} = 5 \times 10^{10}\,cm^{-3}$ and pump current J ($J_{th} \cong 46$ mA)

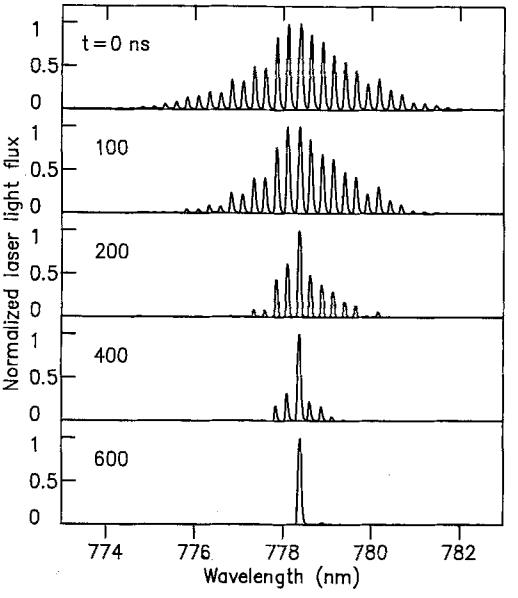

Fig. 6. Normalized diode laser spectra recorded at various delay times t after the onset of laser emission. The time window of detection is 100 ns

structure, and we have tuned a peak of this structure to the position of the Rb absorption by adjusting the diode temperature.

Very strong etalon structure and complete suppression of laser emission at the wavelength of absorption are observed in the spectra recorded above the laser threshold ($J >$ 46 mA). This feature demonstrates the extreme sensitivity of the laser spectrum to ICA. The enhancement of this sensitivity upon increasing the pump current above the threshold shows that the stationary spectrum of the laser, and its sensitivity to ICA, are determined by spontaneous emission, rather than by nonlinear mode interaction, in contrast with dye lasers [3].

Spectra of the diode laser at a constant pump current slightly above threshold, $J = 46$ mA, and at various densities of the intra-cavity absorber, are shown in Fig. 5a–d. ICA suppresses the light flux in the laser spectrum according to the Rb density. Particularly evident is ICA in Fig. 5d, where its line shape forms a dip in the central maximum of the emission. This spectrum shows that each etalon peak consists of many modes of the external cavity and each mode is perturbed independently by the absorber.

In order to estimate the sensitivity of these measurements we have also recorded a single-pass absorption spectrum of Rb at $3 \times 10^{12}\,\mathrm{cm}^{-3}$ density with the absorption cell placed outside the laser cavity. This spectrum is shown in Fig. 5e. It exhibits a similar absorption dip as the spectrum at the intra-cavity Rb density $5 \times 10^{10}\,\mathrm{cm}^{-3}$. Comparison of these spectra shows that at threshold the Rb density inside the laser cavity is 60 times smaller than what is required outside for the same absorption signal. At higher pump current the detection limit is even lower, as demonstrated in Fig. 4.

So far, we have not been able to measure the sensitivity to Rb intra-cavity absorption at higher pump current since an additional modulation shows up in the laser spectrum, which dominates at low Rb densities (Fig. 5a). At the pump currents between 46.5 and 47.0 mA (Fig. 4) this structure grows so strong that the light is quenched at the wavelength of Rb absorption. This modulation probably originates from etalon effects in the lenses and/or windows of the laser cavity, or from irregularities in the diode crystal.

The spectral dynamics of the absorberless laser has been studied when switching the light by the acousto-optical deflectors. Whereas AOD1 is placed inside the laser cavity and switches the feedback, AOD2 sets the 100 ns time window of the spectral recording. Background modulation appears in the spectrum due to the presence of the intra-cavity AOD. Figure 6 shows laser emission spectra up to 600 ns after the onset of laser oscillation at the pump current 1 mA above threshold. Although the temporal resolution is modest only, the spectrum is shown to approach the stationary state within half a microsecond. This is much faster than the transient dynamics in any other multi-mode laser reported so far and is a consequence of the high loss and gain of the laser.

3 Model of the Laser Dynamics

The spectral dynamics of a multi-mode laser and its sensitivity to intra-cavity absorption are described by a model based on rate equations for the number of photons M_q in the cavity mode q, and for the number of inverted states N [3]:

$$\dot{M}_q = -\gamma M_q + B_q N(M_q + 1) - \kappa_q c M_q\,, \tag{3}$$

$$\dot{N} = P - \frac{N}{\tau} - N \sum_q B_q M_q\,. \tag{4}$$

Here, γ is the broad-band cavity loss rate, B_q is the laser gain, $\kappa_q c$ is the narrow-band intra-cavity loss rate, P is the pump rate, and τ is the decay time of the upper laser level. This model applies to ideal four-level lasers, such as dye lasers, Nd^{3+} glass lasers, or colour-centre lasers, since the population of the lower laser level is not taken into account. A semiconductor diode, in contrast, is a two-level laser with a considerable population of the lower state. The application of this model to diode lasers requires modifications, which show up when deriving the probabilities for stimulated and spontaneous recombination of the electron–hole pairs.

The populations of excited and ground states in a semiconductor follow a Fermi-Dirac distribution rather than a Boltzmann distribution as in the broad-band lasers mentioned above. The probability of occupation of a state at the energy E is given by the Fermi-Dirac distribution with the Fermi energy F

$$f(E) = \left[\exp\left(\frac{E-F}{kT}\right) + 1\right]^{-1}, \tag{5}$$

We assume that the semiconductor has a parabolic band structure, $E = \hbar^2 k^2/2m$ (Fig. 7, left), where k is the wave vector and $\hbar k$ is the momentum of the electron or hole, m is the effective mass of electrons in the conduction band ($m = m_c$), and of holes in the valence band ($m = m_v$). In GaAlAs, $m_c = 0.067 m_e$ and $m_v = 0.48 m_e$ [7]. We also assume that all transitions satisfy momentum conservation, $\hbar k = \text{const.}$, as is shown in Fig. 7 (left) by arrows which are labelled by the wavelengths of the transitions. Initial and final energy values $E_1(h\nu)$ and $E_2(h\nu)$ are determined by energy and momentum conservation, $E_2 - E_1 = h\nu$ and

$$m_c(E_2 - E_c) = m_v(E_v - E_1) = m_r(h\nu - E_g)\,, \tag{6}$$

where $m_r = \dfrac{m_v m_c}{m_v + m_c}$ is the reduced mass of an electron, E_v is the maximum energy of the valence band, E_c is the minimum energy of the conduction band, and $E_g = E_c - E_v$ is the energy gap between the bands.

We also assume that the gain of the diode laser is homogeneously broadened, for intraband relaxation in semiconductors is extremely fast (10^{-13} s [7]). Since the rate of transition between the bands is much slower, injection of electrons into the conduction band creates two individual Fermi-Dirac distributions of electrons: f_c in the conduction band, and f_v in the valence band. These distributions differ from each other by their individual quasi-Fermi energies F_c and F_v. Figure 7 (centre) shows these distributions, and the positions of the Fermi energies at the excitation density $n = 2.6 \times 10^{18}\,\mathrm{cm}^{-3}$, which loosely corresponds to the laser threshold.

The densities of states ϱ_c and ϱ_v per energy interval and volume in the conduction and valence bands are shown in Fig. 7 (right); they are expressed as

$$\varrho_c = \frac{\sqrt{2m_c^3}}{\pi^2\hbar^3}(E - E_c)^{1/2}\,;\quad \varrho_v = \frac{\sqrt{2m_v^3}}{\pi^2\hbar^3}(E_v - E)^{1/2}\,. \tag{7}$$

For the calculation of the transition probability, the population densities of electrons in the conduction band, $\varrho_c f_c$, and of holes in the valence band, $\varrho_v(1 - f_v)$, are required. They are shown as functions of energy in Fig. 7 (right). The hatched areas under the population density functions represent the total densities of electrons in the conduction band (n), and of holes in the valence band (p). Since the crystal stays electrically neutral, the overall density of electrons is conserved, hence $p = n$ is valid for arbitrary pumping. This condition defines the Fermi energies F_c and F_v as functions

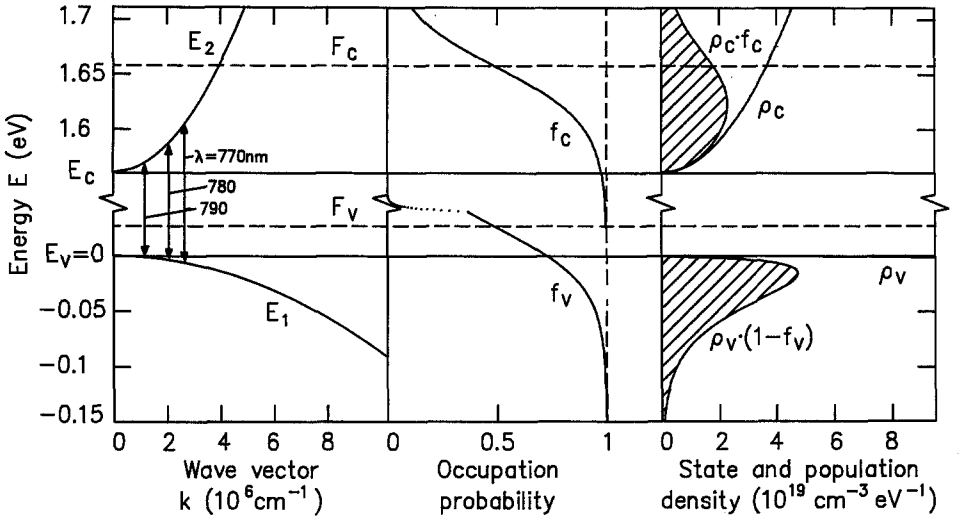

Fig. 7. Dispersion relation of valence (E_1) and conduction (E_2) bands (*left*). Occupation probability f_c and f_v (*centre*) and densities of states and population (*right*) of electrons in the conduction and holes in the valence band of $Ga_{0.89}Al_{0.11}As$ diode with $n = 2.6 \times 10^{18}$ cm^{-3} injected electrons in the conduction band. Optical transitions at wavelength λ are indicated. The hatched areas show the total density of electrons in the conduction band and of holes in the valence band. $E_c = 1.56$ eV is the bottom of the conduction band and $E_v = 0$ is the top of valence band. F_c and F_v are the Fermi energies of electrons in the conduction and valence bands

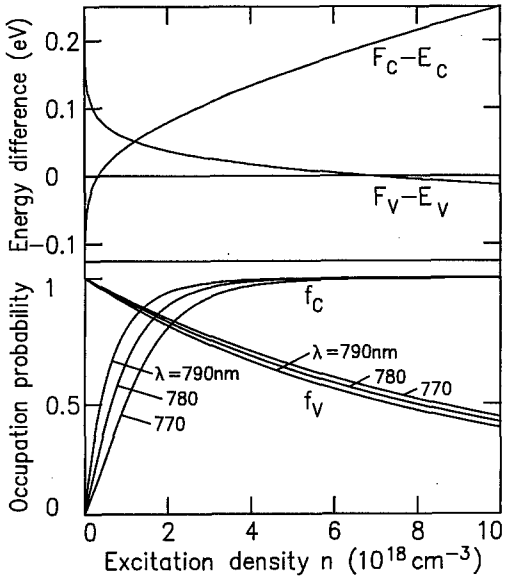

Fig. 8. The Fermi energies F_c and F_v relative to the band origins E_c and E_v (*top*) and the occupation probability in the conduction band (f_c) and in the valence band (f_v), corresponding to transitions with the wavelengths 770 nm, 780 nm, and 790 nm vs the excitation density

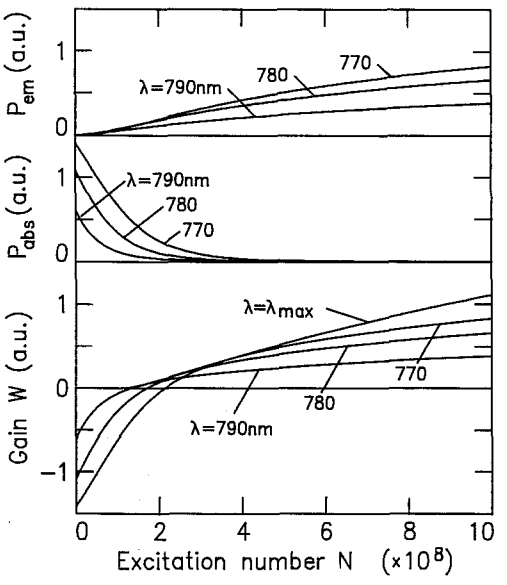

Fig. 9. The spontaneous emission rate in the laser mode P_{em} (*top*), absorptive transition rate P_{abs} (*centre*), and the resulting gain W of the diode laser (*bottom*) vs the excitation number N at three fixed emission wavelengths and at the wavelength λ_{max} of maximum gain

of the excitation density n,

$$\int_{E_c}^{\infty} \varrho_c(E) f_c(E,n)\, dE = \int_{-\infty}^{E_v} \varrho_v(E)\,[1 - f_v(E,n)]\, dE = n\,. \quad (8)$$

The distance of both Fermi energies from the respective band edge vs the density of excited electrons n, obtained with (8), is shown in Fig. 8 (top). Their variation in the excitation range $n = (2\text{–}3) \times 10^{18}$ cm^{-3} is most important. In GaAlAs, the state densities differ considerably, $\varrho_v/\varrho_c = (m_v/m_c)^{3/2} \approx 19$. Therefore, the population of electrons at the bottom of the conduction band saturates at low excitation, $n \approx 10^{18}$ cm^{-3} (Fig. 8, bottom), and the Fermi energy of the electrons moves into the conduction band. The same total population of holes in the valence band is achieved with no major shift of the Fermi energy F_v, which moves into the valence band at ten times the excitation only. Figure 8 (bottom) shows the dependence of the occupation probabilities f_c and f_v upon the excitation rate at the energy levels corresponding to transitions with $\lambda_{em} = 770$ nm, 780 nm, and 790 nm, where $\lambda = 780$ nm is the emission wavelength of the GaAlAs laser to be modeled here.

The rate of spontaneous recombination $P_{em}(h\nu)$ per mode of the electromagnetic field equals the rate of stimulated emission at the same transition per photon in that mode [15] and is the product of five quantities: The first two quantities are the occupation probability $f_c(E_2)$ of the initial energy level E_2 in the conduction band and the probability $1 - f_v(E_1)$ for a hole in the corresponding final energy level E_1 in the valence band. The third quantity is the density of optical transitions per volume and energy interval $h d\nu$,

$$\varrho_r(h\nu) = \frac{\varrho_v \varrho_c}{\varrho_v + \varrho_c} = \frac{\sqrt{2m_r^3}}{\pi^2 \hbar^3} (h\nu - E_g)^{1/2} . \tag{9}$$

The fourth quantity is the transition dipole matrix element μ_{cv}, and the fifth is the fraction of the laser beam that overlaps the active volume of the diode, commonly called the confinement factor Γ. Taking all these factors into account the rate of spontaneously emitted quanta into one mode per unit time is

$$P_{em} = \tilde{B} \Gamma \sqrt{h\nu - E_g}\, f_c(\nu)\,[1 - f_v(\nu)] , \tag{10}$$

where $\tilde{B} = \dfrac{2^{9/2} \pi^3 \nu m_r^{3/2}}{3 n_a^2 \varepsilon_0 h} |\mu_{cv}|^2$ [7], and f_c and f_v depend on the excitation density n via F_c and F_v. For simplicity we have assumed that the lengths of diode and cavity coincide.

Figure 9 (top) shows the calculated rate of spontaneous emission P_{em} vs the total number of excited electron–hole pairs $N = Vn$ at $\lambda_{em} = 770\,\text{nm}$, 780 nm, and 790 nm, where $\lambda = 780\,\text{nm}$ is the emission wavelength of our laser. The active laser volume V is $10^{-10}\,\text{cm}^3$. The emission rate corresponds to the term $B_q N$ in (3). In contrast with the emission rate of a dye laser, P_{em} shows wavelength-dependent saturation and approaches $\tilde{B}\Gamma\sqrt{h\nu - E_g}$. The excitation necessary for the saturation at $\lambda = 780\,\text{nm}$ is determined by the saturation of f_v and amounts to $N = 10^9$.

The rate P_{abs} of absorptive transitions from the valence band to the conduction band per photon and mode is expressed by (10) with f_c and f_v interchanged. Figure 9 (centre) shows P_{abs} vs the number of electrons excited to the conduction band. In contrast with the spontaneous emission rate, P_{abs} saturates together with f_c at the excitation (2–3) $\times 10^8$ already.

The gain W per photon of energy $h\nu$ in the laser mode and per time unit is

$$W = P_{em} - P_{abs} = \tilde{B}\Gamma\sqrt{h\nu - E_g}\,(f_c - f_v); \tag{11}$$

it is shown vs excitation in Fig. 9 (bottom). At low excitation ($0 < f_c < 1$, $f_v \cong 1$) there is absorption, which decreases upon growing excitation until the population of the upper level saturates. At stronger excitation ($f_c \cong 1$, $1 > f_v > 0$), the gain turns positive and is determined by the population of the lower level only. At high excitation $f_c - f_v = 1$, and the gain saturates at the value

$$W_{max}(\nu) = \tilde{B}\Gamma\sqrt{h\nu - E_g} , \tag{12}$$

which increases with the light frequency and equals the rate of linear absorption of the diode without pumping when $f_c - f_v = -1$. However, the light frequency varies only between the band gap values in the active and in the cladding material, and this feature eventually limits the achievable gain. This gain saturation is an important characteristic of the present model. At strong excitation, there is additional gain reduction due to leakage currents.

The explicit inclusion of wavelength-dependent gain and gain saturation characteristically modifies the threshold current density. The variation of this threshold on the thickness d of the active layer is derived by equating the loss γ with (11), $W(\nu, n) = \gamma$. Figure 10 shows this threshold current density vs the width d of the active diode layer. For small d we have used $\Gamma \approx 2\pi^2(n_a^2 - n_c^2)(d/\lambda)^2$ [7] and assumed that the loss does not depend on Γ. Thickness and threshold current density are normalized to the values of our laser, $d \approx 0.1\,\mu\text{m}$ and $j_{th} \approx 5\,\text{kA/cm}^2$. Curve *a* is the result of the previous model [7] which includes *unsaturated* linear gain only. The calculations of the threshold based on the present model are also shown: Curve *c* represents the result calculated with constant emission wavelength $\lambda = 780\,\text{nm}$, which matches a laser with a wavelength-selective element placed in the cavity. Curve *b* corresponds to a broad-band laser, where the threshold relates to the wavelength of maximum gain, λ_{max} (see Fig. 9), which decreases upon growing excitation within the accessible range. We have extended this range from the band gap down to 750 nm which seems realistic for the present laser. The data of Fig. 10 show that the threshold current density diverges once the laser thickness

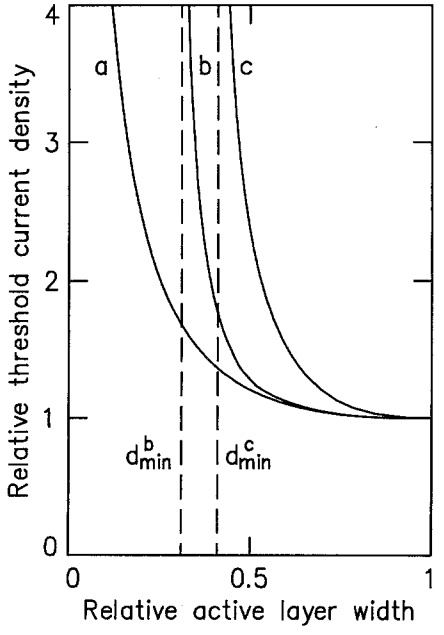

Fig. 10. The threshold current density of the diode laser vs the thickness d of the active layer, calculated with the assumption of unsaturated gain *(a)*, with the present model including gain saturation with $\lambda \geq 750\,\text{nm}$ *(b)*, and at the constant wavelength of emission 780 nm *(c)*. At the asymptotic values d^b_{min} and d^c_{min} the threshold diverges

approaches the value

$$d_{\min} = \left(\frac{\gamma \lambda^2}{2\pi^2 (n_a^2 - n_c^2) B (h\nu - E_g)^{1/2}} \right)^{1/2} . \quad (13)$$

Previous experimental data suggest the existence of such a minimum width of the diode layer, although the matching models lacked it [7, 9, 16, 17].

The spontaneous emission rate P_{em} is a crucial quantity for the calculation of laser spectra and for the definition of their sensitivity fo ICA [1, 3]. The ratio of this rate and the gain per photon is, from (10, 11),

$$\xi_0 = P_{em}/W = \left[1 - \exp\left(\frac{h\nu - (F_c - F_v)}{kT} \right) \right]^{-1} . \quad (14)$$

Figure 11 (top) shows ξ_0 as a function of the excitation for three fixed wavelengths and for the variable wavelength λ_{max} of the gain maximum. At strong excitation, when the absorptive transition rate P_{abs} vanishes, this ratio approaches unity, as it is always the case in a four-level dye laser. Previous models have included spontaneous emission as a phenomenological factor β_{spon} [7, 16, 18, 19], the fraction of fluorescence in a laser mode, which is 10^{-5}–10^{-3}, and whose value was determined such as to fit the experimental data. In contrast, (14) models spontaneous emission as a function of the excitation.

The maximum gain for a laser mode approximates a linear function of excitation N (see Fig. 9, bottom),

$$W \cong B(N - N_t) , \quad (15)$$

with N_t being a constant, the "transparency excitation" [20, 21]. Note that this quantity significantly deviates from the constant excitation, defined by $f_c = f_v$, at which the maximum gain approaches zero, whereas $N_t = N - W(dW/dN)^{-1}$ varies with excitation N. The applicability of the linear approximation in (15) is evaluated in Fig. 11 (bottom), where N_t is shown as a function of excitation N for three fixed wavelengths and for the wavelength of the gain maximum. In a limited range of excitation around laser threshold, N_t can be considered constant. This linearization is inherent to previous models [7, 16, 20, 21]. Here, the error which it introduces is easily determined.

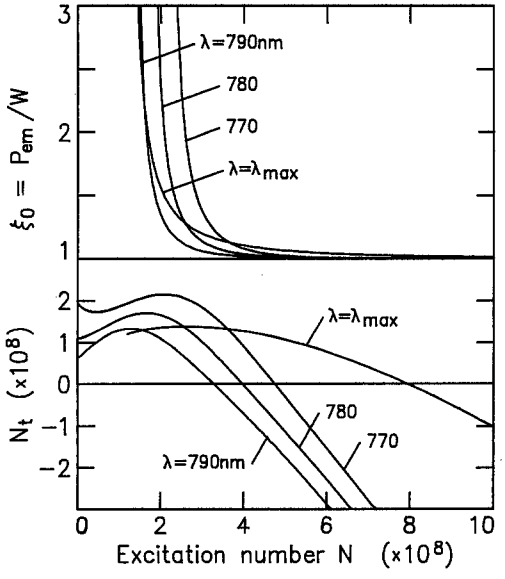

Fig. 11. The relative rate of spontaneous emission (*top*) and the "transparency excitation" N_t (*bottom*) vs excitation N at three emission wavelengths and at the wavelength λ_{max} of maximum gain

So far we have always assumed uniform distribution of loss and gain along the laser cavity. In fact, a large fraction of the loss takes place at the diode facets with the light flux being exponentially amplified between them [9, 21, 22]. As a consequence, the light flux and the gain, which is saturated by this flux, vary spatially, and the output coupling θ, which is the ratio of the output power to the *average* power inside the cavity, deviates from the transmission of the output mirror. These conditions are taken into account in the rate equations. The necessary corrections are found when comparing the solutions of rate equations with solutions of the model based on the Fabry-Perot approach [23] that takes into account the nonuniform distribution of laser loss (see Appendix). This comparison shows that rate equations provide adequate results if the rate of spontaneous emission ξ_0 is increased by a factor k, which, above threshold, depends only on the transmittance of the output mirror R_2 and on the feedback from the external mirror R_1, but neither on the pumping rate nor on the spectral position of the laser mode. For our laser with $R_1 = R_2 = 0.32$ we find $k = 1.11$ and replace ξ_0 by $\xi = k\xi_0$. The output coupling θ is also a function of R_1 and R_2. With $R_1 = R_2 = 0.32$ we get for our laser $\theta = 1.14$.

The complete rate equations (3, 4) for the diode laser with ICA are

$$\dot{M}_q = -\gamma M_q + B_q (N - N_t)(M_q + \xi) - \kappa_q c M_q , \quad (16)$$

$$\dot{N} = P - \frac{N}{\tau} - (N - N_t) \sum_q B_q M_q . \quad (17)$$

The values B_q which we use in the model are derived from experimental data and include the confinement factor Γ. We should like to stress that the rate equations (16) and (17) are written for total numbers of photons and excitations in the cavity in contrast with most other models which use densities of these values and account for the confinement factor in a more complicated way.

4 Calculation of the Spectrum of Diode Laser Emission

In order to calculate laser spectra from (16) and (17) we have to find the operational parameters of our laser. For this purpose we use the observed data of Fig. 3 and fit them on stationary solutions of the rate equations for the total laser power above threshold, assuming spectrally independent gain, $B_q = B_0$, and neglecting narrowband loss, $\kappa_q = 0$,

$$\sum_q M_q = \frac{(\eta - 1)(1 + n_t)}{B_0 \tau} ,$$
$$I_{out} = \theta h\nu (c/2L) \sum_q M_q . \quad (18)$$

Here η is the normalized pump rate $\eta = P/P_{th}$, and $n_t = B_0 N_t/\gamma$ is the absorptive loss over the cavity loss. The threshold pump rate P_{th} is defined as the excitation rate whose emission compensates the cavity loss, $B_0(N - N_t) = \gamma$, namely

$$P_{th} = \alpha J_{th}/e = \frac{\gamma}{B_0\tau}(n_t + 1). \tag{19}$$

Here J is the injection current, e is the electron charge and α is the internal quantum efficiency, defined as the ratio of the light flux (in photons per second) emitted by the diode and the injection current in electrons per second.

Equations (18) and (19) include four laser parameters γ, $B_0\tau$, n_t, and α, which are found from the experimental data shown in Fig. 3. We determine the threshold current $J_{th} = \gamma e(n_t+1)/\alpha B_0\tau$ and the slope efficiency $S = \theta h\nu c\alpha/2L\gamma e$ vs the cavity loss $\gamma = \gamma_0 + \gamma_f$, where $\gamma_f = (-c/L)\ln(T_f)$ is the additional loss by the filter of transmittance T_f inserted into the cavity. The slope efficiency is calibrated making use of the data supplied by the manufacturer, i.e. $S = 0.292\,\mathrm{mW/mA}$ at 25° C temperature. Linear approximations to J_{th} and θ/S vs γ_f, shown in Fig. 12, yield the quantities J_{th}^0 and θ^0/S^0, for $\gamma_f = 0$, and $dJ_{th}/d\gamma = e/\alpha B_0\tau$ and $d(\theta/S)/d\gamma = 2Le/h\nu c\alpha$. The output coupling coefficient θ is calculated for each level of loss according to the procedure given in the Appendix. We find $dJ_{th}/d\gamma = 2.1 \times 10^{-11}\,\mathrm{As}$ and $d(\theta/S)/d\gamma = 3.8 \times 10^{-9}\,\mathrm{AsW^{-1}}$. The laser parameters are related to these experimental data as

$$\alpha = \frac{2Le}{h\nu c}\left(\frac{d(\theta/S)}{d\gamma}\right)^{-1}, \tag{20}$$

$$B_0\tau = \frac{\theta h\nu c}{2L}\frac{d(\theta/S)}{d\gamma}\left(\frac{dJ_{th}}{d\gamma}\right)^{-1}, \tag{21}$$

$$n_t = \frac{J_{th}^0 S^0}{\theta^0}\frac{d(\theta/S)}{d\gamma}\left(\frac{dJ_{th}}{d\gamma}\right)^{-1} - 1, \tag{22}$$

$$\gamma_0 = \frac{\theta^0}{S^0}\left(\frac{d(\theta/S)}{d\gamma}\right)^{-1}. \tag{23}$$

For our laser whose length is $L = 72\,\mathrm{cm}$ we obtain $\alpha = 0.77$, $B_0\tau = 9.6\times10^{-9}$, $n_t = 1.2$, $\gamma_0 = 1.0\times10^9\,\mathrm{s^{-1}}$. Since the spontaneous lifetime τ is about 1 ns [24], we estimate $B_0 \approx 10\,\mathrm{s^{-1}}$. The total broad-band cavity loss γ_0 consists of the output coupling $\gamma_e = (-c/2L)\ln(R_0R_1) = 4.8\times10^8\,\mathrm{s^{-1}}$ and the internal scattering and absorption loss, which is $\gamma_i = \gamma_0 - \gamma_e = 5.2\times10^8\,\mathrm{s^{-1}}$. The internal loss γ_i is rather high and determined by the imperfections of the diode.

In the definition of the laser threshold (19) we have assumed the laser gain to equal the loss. Exact stationary solutions of the rate equations

$$M_q = \frac{B_q(N - N_t)\xi}{\gamma_q - B_q(N - N_t)}, \tag{24}$$

$$N - N_t = \frac{P\tau - N_t}{1 + \tau\sum_q B_q M_q}, \tag{25}$$

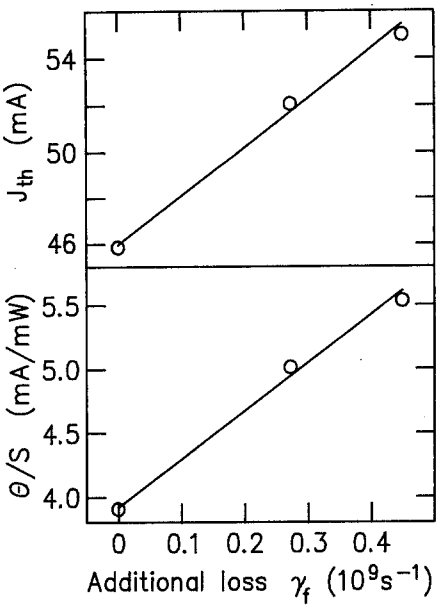

Fig. 12. The threshold current and the inverse of the slope efficiency of the diode laser, normalized by the output coupling θ, θ/S, vs the additional loss γ_f in the cavity

(where $\gamma_q = \gamma_0 + \kappa_q c$) show that the laser gain is always smaller than the loss. The difference, which is the contribution of spontaneous emission to the total laser power, is expressed by the inversion factor ε [9] defined as

$$N - N_t = \frac{\gamma_0}{B_0}(1 - \varepsilon). \tag{26}$$

We set $q = 0$ at maximum emission which is located, according to (25), at the minimum of γ_q/B_q.

The factor ε can be used as a new variable in the rate equations instead of the laser inversion $N - N_t$. It is a convenient parameter for evaluating stationary laser spectra and their sensitivity to ICA. Equations (24) and (25) are rewritten as

$$M_q = M_0\left[1 + \frac{1}{\varepsilon}\left(\frac{B_0\gamma_q}{B_q\gamma_0} - 1\right)\right]^{-1}, \quad M_0 = \xi\frac{1-\varepsilon}{\varepsilon}, \tag{27}$$

$$(1 - \varepsilon)\tau\sum_q B_q M_q = (\eta - 1)(1 + n_t) + \varepsilon. \tag{28}$$

M_q and ε are numerically calculated from these equations as functions of η. Not too close to threshold, $|\eta - 1| \geq 0.02$, approximate solutions for ε are

$$\varepsilon(\eta < 1) \approx (1 - \eta)(1 + n_t), \tag{29}$$

$$\varepsilon(\eta > 1) \approx \frac{\xi B_0\tau}{(1 + n_t)(\eta - 1)}m, \tag{30}$$

where $m = \sum_q \frac{M_q}{M_0}$ is the effective number of oscillating modes. Below threshold ε decreases linearly with the pump rate from $n_t + 1$ to almost 0. Above threshold, $0 < \varepsilon \ll 1$, the total laser power can be approximated by (18).

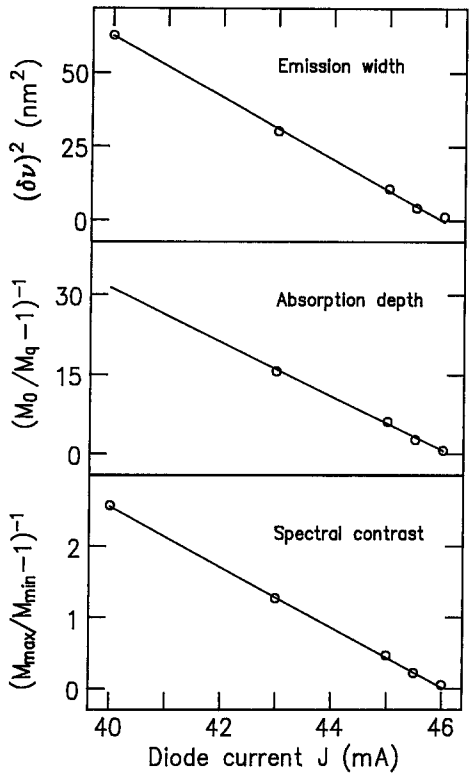

Fig. 13. The emission linewidth, the absorption dip in the spectrum caused by intra-cavity Rb absorption, and the modulation depth of channelling vs pump current

Now we calculate the laser spectrum when the gain depends on the frequency. We assume that the gain has a Lorentzian spectral profile of width $\Delta\nu$ (HWHM), although the precise shape of the gain spectrum is unimportant since only the curvature of the gain at its maximum determines the shape of the laser spectrum. From (27) we see that the envelope of the emission spectrum is also Lorentzian with the width

$$\delta\nu = \Delta\nu\sqrt{\varepsilon}\,. \tag{31}$$

Below threshold ε is expressed by (29) and the bandwidth of emission is

$$\delta\nu = \Delta\nu\sqrt{(1-\eta)(1+n_t)}\,. \tag{32}$$

The square of the observed spectral bandwidth of the diode laser emission below threshold is shown vs the pump current in Fig. 13. The bandwidth of the gain is derived from the linear fit according to (32) by extrapolating $\delta\nu$ to $\eta = 0$ as $\Delta\nu/c = \delta\nu_0(1+n_t)^{-1/2}/c = 240\ \mathrm{cm}^{-1}$ (HWHM).

The same procedure is used for deriving the value of the spectrally varying fraction κ_q of the loss. We assume that the spectral width of this loss is much smaller than the laser emission bandwidth. If this loss is situated in the vicinity of the emission maximum, we can furthermore assume $B_q \approx B_0$. Using (27) and (29), the residual emission over the suppression of laser output in mode q, which we define as the spectral contrast, is

$$\left(\frac{M_0}{M_q}-1\right)^{-1} = \frac{\varepsilon\gamma_0}{c\kappa_q} = (1-\eta)(1+n_t)\frac{\gamma_0}{c\kappa_q}\,. \tag{33}$$

The extrapolation of the spectral structure in the laser emission to zero pump rate ($\eta = 0$) gives the absolute value of the loss difference between mode q and 0, averaged over the cavity length,

$$\kappa_q = \frac{\gamma_0}{c}(1+n_t)\left(\frac{M_0}{M_q}-1\right)_{\eta=0}\,. \tag{34}$$

The frequency-dependent loss κ_q in the cavity of our laser consists of the intra-cavity line absorption and a spectrally periodic loss due to interference which results from the imperfect AR coating of the diode facet.

The depth of the absorption line of Rb in the laser spectrum at the density $5 \times 10^{10}\,\mathrm{cm}^{-3}$ vs pump rate is shown in Fig. 13 (centre). Extrapolation of the linear fit to $J = 0$ gives the value of the absorption coefficient at the centre of the Rb line $\kappa_q = 2.3 \times 10^{-4}\,\mathrm{cm}^{-1}$. This value corresponds to the optical density $D = \kappa_q L = 1.7 \times 10^{-2}$ of the absorption cell at resonance. This estimate is checked by comparison with the spectrum of single-pass absorption at the Rb concentration of $3 \times 10^{12}\,\mathrm{cm}^{-3}$ (Fig. 5e) and $D_0 = 1.14$. The ratio of the optical densities $D_0/D = 67$ agrees well with the ratio 60 of the atomic densities.

Interference in the three-mirror cavity can be treated as an equivalent loss by substituting in the expression for the coupling loss, $\gamma_e = (-c/2L)\ln(R_1R_2)$, for R_1 the effective reflectivity R_{eff} of both the coated facet with residual reflectivity R and the external mirror [25], calculated to first order in r/r_1,

$$R_{\mathrm{eff}} = |r_1 + r\,\mathrm{e}^{\mathrm{i}\varphi} - rr_1^2\,\mathrm{e}^{-\mathrm{i}\varphi}|^2\,, \tag{35}$$

where $r_i = \sqrt{R_i}$ and φ is the round-trip phase of a laser mode in the diode crystal. The resulting periodic variation of the cavity loss is

$$\kappa_q \approx \frac{2}{L}(1-R_1)\sqrt{R/R_1}\sin^2(\pi ql/L)\,, \tag{36}$$

where l is the length of the diode crystal. This approximation agrees within 2% with the exact solution, based on the determination of the complex roots of the denominator which appears in the transmission or reflection coefficient of the cavity [15]. We use this approximation for an estimate of the residual reflectivity of the coated facet. This quantity can be expressed with (34) and (36) by the contrast ratio of the interference structure in the laser spectrum, extrapolated to $\eta = 0$

$$R = R_1\left[\frac{\gamma_0 L(1+n_t)}{2c(1-R_1)}\left(\frac{M_{\max}}{M_{\min}}-1\right)_{\eta=0}\right]^2. \tag{37}$$

Experimental data on the contrast of the spectral modulation vs pump rate and a linear fit are shown in Fig. 13 (bottom). Extrapolation of the linear fit to $\eta = 0$ gives $(M_{\max}/M_{\min}) - 1 = 0.051$ and $R = 0.012$. The residual reflectivity of the AR coating of our diode turns out to be $R = 1.2\%$. This method for the determination of the rest reflectivity of the diode laser is more precise than the method based on the measurement of the spectral modulation of the diode emission at the original threshold pump current [13], which has been mentioned before.

The same procedure, when applied to the spectra recorded at very low absorber density, gives the spectrally varying background loss, which is superimposed on the Rb absorption and which limits the sensitivity of detection. In our experiment this loss variation is $\kappa_q = 1 \times 10^{-4}\,\mathrm{cm}^{-1}$ with $6.3\,\mathrm{cm}^{-1}$ spectral width.

Stationary laser spectra have been modeled from (27, 28) taking into account the spectral variation of gain, intracavity Rb absorption at $N_{\mathrm{Rb}} = 5 \times 10^{10}\,\mathrm{cm}^{-3}$, interference structure due to imperfect AR coating, and the background loss determined above. Equations (27, 28) are most easily solved for a given value of the inversion factor ε. To calculate the spectrum from (27) for a given pump rate η, the appropriate value of ε is found iteratively. Comparison of the calculated spectra with the experimental results makes one find the experimental laser threshold $J_{\mathrm{th}}^0 = 45.9\,\mathrm{mA}$ with better precision and estimate the relative spontaneous emission rate above threshold $\xi = 2$.

Figure 14 shows the results of the numerical calculations for the pump rates corresponding to the observed spectra in Fig. 4. Comparison reveals that the calculated spectra reproduce all the features of the experiment mentioned in Sect. 2. The increase of the sensitivity with the pump rate above threshold confirms the basic assumption of the model, namely the stationary spectrum of the diode laser and its sensitivity to ICA being determined by spontaneous emission. This is in contrast with dye lasers, whose spectra (and sensitivity) are determined by nonlinear mode coupling and where the sensitivity decreases with the pump rate [26].

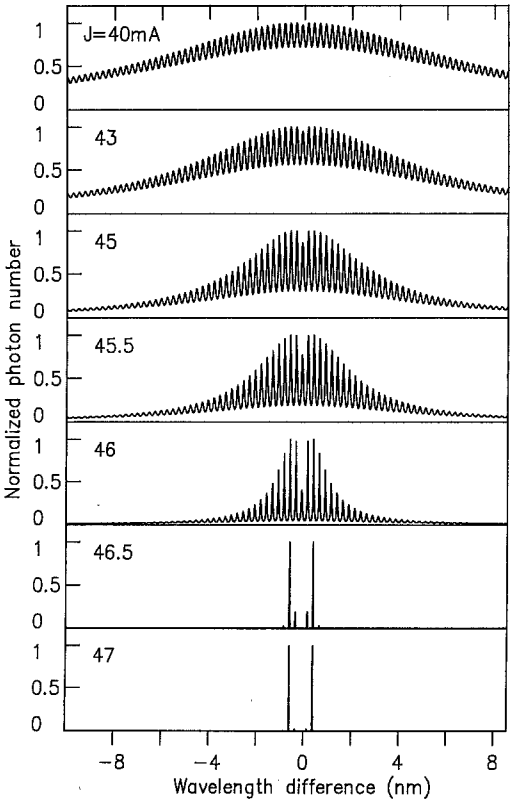

Fig. 14. Calculated emission spectra of the diode laser with intra-cavity absorption of Rb at density $N = 5 \times 10^{10}\,\mathrm{cm}^{-3}$ and pump current J

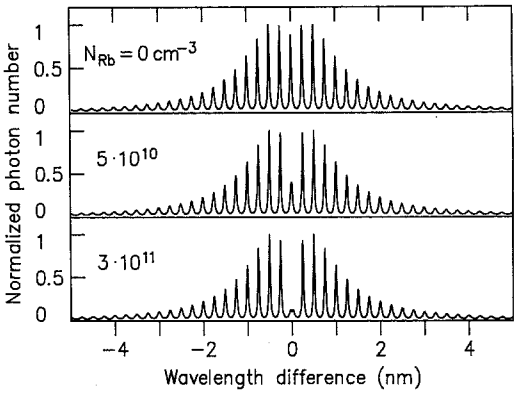

Fig. 15. Calculated emission spectra of the diode laser at the constant pump current $J = 46\,\mathrm{mA}$ and various absorber densities N_{Rb} in the laser cavity

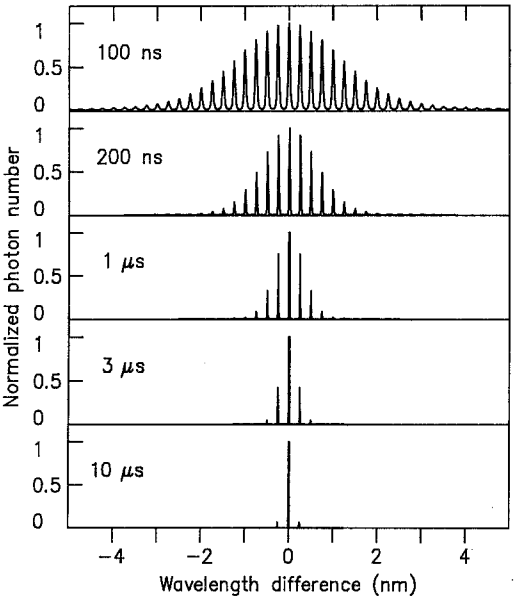

Fig. 16. Calculated time-resolved spectra of the laser emission at relative pump rate $\eta = 1.02$ and with various delay times after switching the laser on

Figure 15 shows laser spectra calculated with the pump rate that corresponds to $J = 46\,\mathrm{mA}$, and for various densities of the intra-cavity absorber, which match the values in Fig. 5. The results of the model again reproduce the expeirmental data. The sensitivity of the detection of Rb atoms in our experimental setup is limited by the background spectral loss structure in the spectrum. This limit approximately corresponds to the Rb density $N_{\mathrm{Rb}} = 2 \times 10^{10}\,\mathrm{cm}^{-3}$, i.e. to the absorption coefficient of $10^{-4}\,\mathrm{cm}^{-1}$.

We have also calculated transient emission spectra of the diode laser, at various delay times after switching on the laser, by integrating the rate equations (16) and (17). This integration was made with adiabatic elimination of the laser inversion. Equations (16) have been integrated, in steps of $10^{-11}\,\mathrm{s}$ duration, for 60000 laser modes. We have assumed the same Lorentzian spectral profile of the gain and the same interferometric structure due to imperfect AR coating as in the previous calculations, but no ICA

and no background loss. Corresponding to the experimental conditions of the spectra in Fig. 6 (where the laser was switched by the AOD1), the initial spectrum was calculated for the steady state with $\eta = 0.9$. At $t \geq 0$, the pump parameter was assumed to be $\eta = 1.02$. The time evolution of the spectrum is shown in Fig. 16. It shows reduction of the emission bandwidth at $t^{-1/2}$ and an exponential increase of the interference structure. The stationary spectrum, which appears after about 10 µs, corresponds to the spectra in Fig. 14 with no absorption. In the recordings of Fig. 6, the stationary spectrum is reached at earlier times. This discrepancy with the calculated spectra may result from the spectral variation of the background loss and from the presence of the AOD in the cavity.

The agreement of the experimental and numerical results below and above threshold confirms our model and allows us to estimate the sensitivity limits of an intra-cavity diode-laser spectrometer to ICA under various conditions of operation.

5 Sensitivity

Detection of absorption with the reported experiment is limited by imperfections of the setup, which give rise to spurious spectrally varying background loss. On the other hand, the fundamental limit of the sensitivity is determined by spontaneous emission. The model outlined above allows us to calculate the sensitivity and its limit. We define the limit of detection that determines the sensitivity of ICA measurements as the absorption coefficient $\kappa_{\min}$, which reduces the spectral density of the laser flux by 50% in the center of the stationary laser emission spectrum. We further assume that the absorption bandwidth is small as compared with the emission bandwidth so that only a small fraction of the emitting modes is affected by ICA. The width of absorption should exceed the mode spacing, however, and overlap at least with one laser mode. From (27) or (33) the detection limit is

$$\kappa_{\min} = \gamma_0 \varepsilon / c, \tag{38}$$

determined by the broad-band cavity loss γ_0 and the inversion factor ε. Increasing the pump rate results in a smaller value of ε and in the detection of smaller absorption coefficients. Above threshold the sensitivity is expressed with (30) and (38) as

$$\kappa_{\min} = \frac{\gamma_0 \xi B_0 \tau m}{c(\eta - 1)(n_t + 1)}. \tag{39}$$

Note that the number of oscillating modes (m) determines the sensitivity for ICA. This number critically depends on the residual reflectivity R, which causes spectral modulation. Therefore, we first estimate $\kappa_{\min}$ for the diode laser with no modulation, i.e. with $R = 0$.

In certain lasers, e.g., with inhomogeneously broadened gain, as in the Nd-glass laser [1], the number of oscillating modes (m) does not depend upon the pump rate, and, according to (39), the detection limit is inversely proportional to $(\eta - 1)$. If the gain is homogeneously broadened and its profile is Lorentzian, the width of the laser emission spectrum decreases with the pump rate and the number of oscillating modes $m = \pi \delta \nu 2L/c$ is derived from (30) and (31),

$$m = \frac{\xi B_0 \tau}{(n_t + 1)(\eta - 1)} \left(\frac{2\pi L \Delta \nu}{c} \right)^2. \tag{40}$$

With (39) the detection limit is

$$\kappa_{\min} = A \frac{\gamma_0}{(\eta - 1)^2}, \tag{41}$$

where $A = (1/c)[\pi \Delta \nu 2LB_0 \tau \xi / c(n_t + 1)]^2$. For the diode laser with $\Delta \nu / c = 240\,\mathrm{cm}^{-1}$, $L = 72\,\mathrm{cm}$, $B_0 \tau = 9.6 \times 10^{-9}$, $\xi = 2$, $n_t = 1.2$, and $\gamma_0 = 1 \times 10^9\,\mathrm{s}^{-1}$, we obtain $A = 3.0 \times 10^{-17}\,\mathrm{s/cm}$ and $\kappa_{\min} = 3.0 \times 10^{-8}/(\eta - 1)^2\,\mathrm{cm}^{-1}$. For the maximum allowed pump rate $\eta = 1.2$, $\kappa_{\min} = 7.5 \times 10^{-7}\,\mathrm{cm}^{-1}$.

Equation (41) also holds for a dye laser with uncoupled modes. For a cw rhodamine 6G laser with $\Delta \nu \approx 1000\,\mathrm{cm}^{-1}$, $\tau = 6 \times 10^{-9}\,\mathrm{cm}^{-1}$ [27], $B_0 = 0.01\,\mathrm{s}^{-1}$ [28], $\xi = 1$, and $n_t = 0$, we obtain $A = 2.5 \times 10^{-20}\,\mathrm{s/cm}$, some 10^3 times smaller than with the diode laser. Furthermore, the broadband loss in the cavity of a dye laser, $\gamma_0 \approx 10^7\,\mathrm{cm}^{-1}$, is 100 times smaller and the operational pump rate excess $\eta - 1 \approx 1$ is 10 times higher. As a result, the expected detection limit of an ICA measurement with a dye laser is some 10^7 times below that with a diode laser, when the modes oscillate continuously and uncoupled. Mode coupling reduces the sensitivity of a dye laser to about $10^{-9}\,\mathrm{cm}^{-1}$ [26]. In contrast, mode coupling in diode lasers has not yet been observed.

Figure 17 shows the detection limit $\kappa_{\min}$ of the diode laser intra-cavity spectrometer and the inversion factor ε vs pump rate calculated with (38). The two quantities drop at threshold by some orders of magnitude.

Spurious channelling in the diode laser spectrum results in a drastic reduction of the number of oscillating modes down from (40). The laser spectrum consists of several mode groups or "channels". Both the number of channels and the number of modes in each channel decrease with

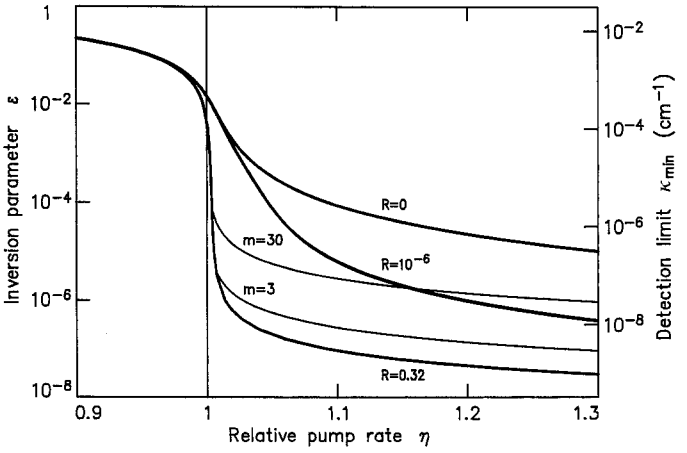

Fig. 17. The detection limit $\kappa_{\min}$ and the inversion factor ε vs pump parameter $\eta = J/J_{th}$ at various values of the residual reflectivity R of the diode facet. The number of oscillating modes is m

increasing pump rate, giving rise to an approximately inverse square dependence of m vs $(\eta - 1)$ in contrast with the simple inverse dependence in (40). Finally, the detection limit depends as an inverse cubic upon the pump rate, $\kappa_{\min} \sim (\eta - 1)^{-3}$, as is seen in Fig. 17 in the curve calculated for $R = 10^{-6}$. Upon increasing η above threshold, the detection limit drops faster at $R = 10^{-6}$ than at $R = 0$. When $\eta > 1.1$, the graphs of $\kappa_{\min}$ for $R = 0$ and for $R = 10^{-6}$ turn parallel: For $R = 10^{-6}$ only one maximum of the interferometric structure is left over in the emission spectrum and the other maxima are suppressed because of their low gain. The number of modes in the only left-over channel drops, and $\kappa_{\min} \sim (\eta - 1)^{-2}$ as for $R = 0$.

With no AR coating ($R = 0.32$), channelling in the laser spectrum is much stronger and the number of oscillating modes shrinks even more drastically upon increase of pump power.

One may want to relate the number of oscillating modes with the sensitivity limit. Figure 17 shows ε and $\kappa_{\min}$ for the number of modes $m = 3$ and $m = 30$. According to (30), these curves vary as $(\eta - 1)^{-1}$ and separate the parameter space into three regions: multi-mode ($m > 30$), few-mode ($3 < m < 30$) and nearly single-mode ($m < 3$) operation.

Multi-mode operation with $m > 30$ is most important. The channel-free laser ($R = 0$) oscillates in about 500 modes at $\eta \approx 1.2$ with the detection limit $\kappa_{\min} \approx 1 \times 10^{-6}\,\mathrm{cm}^{-1}$. AR coating with 10^{-6} residual reflectivity reduces the number of modes to 10, and, surprisingly, the detection limit drops to $3 \times 10^{-8}\,\mathrm{cm}^{-1}$. This sensitivity only applies if the line width of absorption does not much exceed the mode spacing. For the modeled diode laser the absorption linewidth should be smaller than 500 MHz (2.5 mode spacings). There is a trade-off between the sensitivity and the bandwidth of detection, which can be controlled by spectrally selective loss, i.e. by the residual reflectivity R.

When the laser arrives at single-mode operation, the factor ε keeps decreasing upon growing $\eta - 1$, see (39). However, due to the strong coupling of the single mode and the inversion, the limit of detection $\kappa_{\min}$ does no longer vary as ε and the laser is not very sensitive to ICA. Even in this situation of single-mode ICA spectroscopy [3] we can achieve reasonable sensitivity when the absorption line coincides with the wavelength of the only operating mode and when it is stronger than the difference of the net gain at the frequencies of the oscillating and neighbouring suppressed modes. Additional modes will kindle and mark the transition from single-mode to few-mode operation. Another criterion for the sensitivity is now suitable. It is the condition that the above-mentioned difference of net gain vanishes, and one or more additional modes oscillate with the same amplitude. If the absorption line and the operating mode coincide *at the centre* of the gain profile, the presence of the absorption turns single-mode operation to three-mode operation. When these additional modes are the next modes of the laser this detection limit is $\kappa_{\min} = 1 \times 10^{-7}\,\mathrm{cm}^{-1}$. When the additional modes are located at the next interferometric maximum, the detection limit is $\kappa_{\min} = 1 \times 10^{-5}\,\mathrm{cm}^{-1}$. Both these values are specific for the particular laser used, but independent of the pump rate, once single-mode operation has set in.

6 Summary

We have shown experimentally and theoretically that diode lasers with AR coated facet can be used for multi-mode intra-cavity spectroscopy of high sensitivity. The minimum detectable absorption is determined by the pump rate or, in other words, by the fraction of spontaneous emission in the total emission, and by the broad-band loss. Perfect AR coating and pumping at the maximum rate that is allowed for the present laser sets the limit of detection to $10^{-6}\,\mathrm{cm}^{-1}$, which corresponds to an equivalent of 10 km absorption length.

It should be noted that the model developed in this work can be used for the evaluation of emission spectra and sensitivity to ICA for any type of diode laser, whereas the numerical estimates are tied to the particular laser used. One may expect that technological progress in the manufacturing of diode lasers will cut the internal loss and boost the output, with the benefit of lower detection limits for ICA.

Appendix

The outlined model of the diode laser assumes that loss and gain are uniformly distributed over the entire laser cavity, and hence the spatial photon distribution is also uniform. In fact, a major fraction of loss is localized at the facets, with the light flux exponentially growing inbetween. As a consequence the gain, saturated by the local intensity, varies along the cavity length, and the total photon number in the cavity, calculated by integration of the photon distribution over the length, deviates from the integrated photon density as calculated from a solution of the model equations. Furthermore, the output coupling θ, i.e. the ratio of output power to average power inside the cavity, does not equal the transmission coefficient of the output mirror. These discrepancies can be taken into account by matching the rate equations to the results obtained from the more accurate Fabry-Perot resonator (FPR) approach [23] which includes the real distribution of the cavity loss.

In this approach the laser resonator is characterized by its length, taken to be equal to the optical length of the diode l, by the mirror reflectivities R_1 and R_2, by the frequency-dependent single-pass gain $G(\nu)$, and by the spontaneous emission rate per unit length σ. At a pump rate up to 10% above threshold the gain saturates mainly due to luminescent recombination and carrier diffusion rather than stimulated emission. The variation of laser gain in the diode along the optical axis does not exceed 1% even if the local laser flux varies by several 10% and we approximate the gain as being independent of z. The total cavity loss γ is divided in the external coupling loss γ_e and internal (absorption and scattering) loss γ_i and we can write the relation between the

parameters of the FPR model and the rate equations as

$$\gamma_e = -\frac{c}{2l}\ln(R_1R_2),$$

$$B_q(N-N_t)-\gamma_i = \frac{c}{2l}\ln G^2(\nu_q),$$

and

$$\sigma = \frac{B(N-N_t)\xi_0}{2lc}.$$

The photon numbers per unit length in $+z$ and $-z$ direction ($z=0$ at R_1) are given by

$$I_+(z,R_1,R_2) = \frac{\sigma l}{\ln(G)}\left\{\left[\frac{(G-1)R_2(1+R_1G)}{1-R_1R_2G^2}+1\right]\times\exp[zl^{-1}\ln(G)]-1\right\}, \quad \text{(A1)}$$

$$I_-(z,R_2R_1) = I_+(l-z,R_1,R_2). \quad \text{(A2)}$$

By integration of (A1) and (A2) over the cavity length l we obtain the total photon number M in the FPR and the output coupling θ as functions of R_1, R_2, and G,

$$M = \frac{\sigma l^2}{\ln(G)}\left\{\frac{(G-1)[(1-R_2)(1+R_1G)+(1-R_1)(1+R_2G)]}{\ln(G)(1-R_1R_2G^2)}-2\right\}, \quad \text{(A3)}$$

$$\theta = \frac{(1-R_2)I_-(0)}{M/2l}. \quad \text{(A4)}$$

In the rate equation model the same quantities are given by

$$M^{re} = -\frac{\sigma(2l)^2}{\ln(R_1R_2G^2)}, \quad \text{(A5)}$$

$$\theta^{re} = 1-R_2. \quad \text{(A6)}$$

Evaluation of (A3) and (A5) for the same value of the gain close to threshold, i.e. for $G \approx (R_1R_2)^{-1/2}$, shows that the total laser power in both models differs by $k = M/M^{re}$ which to high accuracy turns to be independent of G. Although G may vary with frequency and pumping rate, the constant ratio k applies to all the spectra near and above threshold. Figure 18 (top) shows k vs the external feedback R_1, for constant $R_2 = 0.32$. For the experiment where $R_1 = 0.32$ we get $k = 1.11$, which means that, with equal parameter values, the rate equations would predict lower average power per mode than the FPR model. This discrepancy is eliminated (see (A5)) by increasing the spontaneous emission rate in the rate equations by the factor k, i.e. ξ_0 be replaced by $\xi = 1.11\xi_0$, such that at equal pump rate, both the total laser power and the spectrum are equal in the two models. Physically, the enhancement of the spontaneous emission is explained by the delay between the emission and loss processes. The spontaneously emitted light is amplified during its propagation towards the facet. This effect is described as an equivalent enhancement of the spontaneous emission [9, 19, 29].

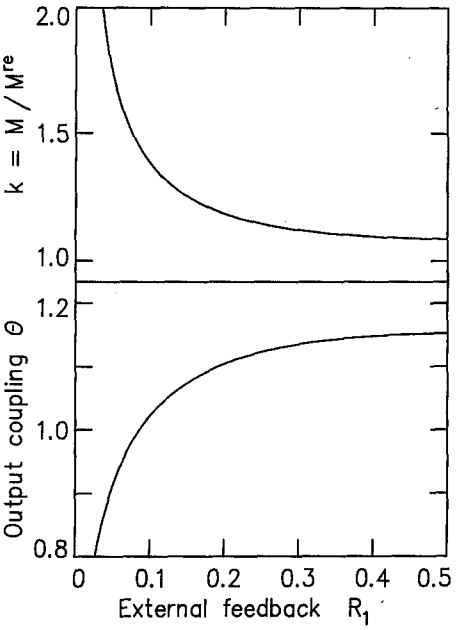

Fig. 18. The ratio k of the light flux in the laser cavity calculated by a FPR approach and the flux calculated by rate equations with equal parameters (*top*), and the output coupling θ (*bottom*) vs the external feedback R_1

Likewise, the output coupling θ does not depend on the pump rate when $G \approx (R_1R_2)^{-1/2}$. For our diode crystal with one uncoated facet ($R_2 = 0.32$) θ depends only on the external feedback R_1, as shown in Fig. 18 (bottom). With $R_1 = R_2$, $\theta = 1.14$. This value is required for calculating the total laser power in the cavity from the measured output power.

With these corrections included, the laser rate equations take into account the nonuniform distribution of the cavity loss and provide correct results for emission spectrum and gain of the laser.

Acknowledgements. This work was supported by the "Deutsche Forschungsgemeinschaft". – J.E. acknowledges a grant by the "Studienstiftung des Deutschen Volkes".

References

1. L.A. Pakhomycheva, E.A. Sviridenkov, A.F. Suchkov, L.V. Titova, S.S. Churilov: Line structure of generation spectra of lasers with inhomogeneous broadening of the amplification line. JETP Lett. **12**, 43–45 (1970)
2. T.W. Hänsch, A.L. Schawlow, P.E. Toschek: Ultrasensitive response of a cw dye laser to selective extinction. IEEE J. QE-**8**, 802–804 (1972)
3. P.E. Toschek, V.M. Baev: One is not enough. Intracavity spectroscopy with multi-mode lasers. In *Lasers, spectroscopy and new ideas*, ed. by W.M. Yen, M.D. Levenson, Springer Ser. Opt. Sci., Vol. 54 (Springer, Berlin, Heidelberg 1987) pp. 89–111
4. G. Eisenstein, L.W. Stultz: High quality antireflection coating on laser facets by sputtered silicon nitride. Appl. Opt. **23**, 161–164 (1984)
5. W. Rideout, R. Holmstrom, J. Lacourse, E. Meland, W. Powazinik: Ultra-low-reflectivity semiconductor optical amplifiers without antireflection coatings. Electron. Lett. **26**, 36–38 (1990)

6. Hitachi Optodevice Data Book. Semiconductor and IC Div. Hitachi, Ltd. (1989)
7. K.J. Ebeling: *Integrierte Optoelektronik* (Springer, Berlin, Heidelberg 1989)
8. H.C. Casey, Jr., D.D. Sell, M.B. Panish: Refractive index of AlGaAs between 1.2 and 1.8 eV. Appl. Phys. Lett. **24**, 63 (1974)
9. G.H.B. Thompson: *Physics of Semiconductor Laser Devices* (Wiley, Chichester 1980)
10. D.R. Kaplan, P.P. Deimel: Exact calculation of the reflection coefficient for coated optical waveguide devices. AT & T Bell Syst. Tech. J. **63**, 857–877 (1984)
11. T. Saitoh, T. Mukai, O. Mikami: Theoretical analysis and fabrication of antireflection coatings on laser diode facets. IEEE J. LT-**3**, 288–293 (1985)
12. M. Serenyi, H.-U. Habermeier: Directly controlled deposition of antireflection coatings for semiconductor lasers. Appl. Opt. **26**, 845–849 (1987)
13. I.P. Kaminow, G. Eisenstein, L.W. Stulz: Measurement of the modal reflectivity of an antireflection coating on a superluminescent diode. IEEE J. QE-**19**, 493–495 (1983)
14. W. Demtröder: *Laser Spectroscopy*, Springer Ser. Chem. Phys., Vol. 5 (Springer, Berlin, Heidelberg 1988)
15. A.E. Siegman: *Lasers* (University Science Books, Mill Valley, CA 1986)
16. E. Kapon: Semiconductor diode laser: Theory and techniques, In *Handbook of Solid-State Lasers*, ed. by P.K. Cheo (Dekker, New York 1989)
17. O. Svelto, D.C. Hanna: *Principles of Lasers* (Plenum, New York 1989)
18. Y. Suematsu, S. Akiba, T. Hong: Measurement of spontaneous-emission factor of AlGaAs double-heterostructure semiconductor lasers. IEEE J. QE-**13**, 596–600 (1977)
19. K. Petermann; Calculated spontaneous-emission factor for double-heterostructure injection lasers with gain-induced waveguiding. IEEE J. QE-**15**, 566–570 (1979)
20. M. Port, K.J. Ebeling: Intensity noise dependence on the injection current of laser diodes with optical feedback. IEEE J. QE-**26**, 449–455 (1990)
21. K.Y. Lau, A. Yariv: A theory of longitudinal modes in semiconductor lasers. Appl. Phys. Lett. **40**, 763–765 (1982)
22. D.T. Cassidy: Analytic description of a homogeneously broadened injection laser. IEEE J. QE-**20**, 913–918 (1984)
23. D.T. Cassidy: Comparison of rate-equation and Fabry-Perot approaches to modeling a diode laser. Appl. Opt. **22**, 3321–3326 (1983)
24. H.C. Casey, F. Stern: Concentration-dependent absorption and spontaneous emission of heavily doped GaAs. J. Appl. Phys. **47**, 631–643 (1976)
25. M.J. Adams, J. Buus: Two-segment cavity theory for mode selection in semiconductor lasers. IEEE J. QE-**20**, 99–103 (1984)
26. Yu.M. Aivazyan, V.M. Baev, V.V. Ivanov, S.A. Kovalenko, E.A. Sviridenkov: Kinetics of emission spectra of multimode lasers and its influence on the sensitivity of intracavity laser spectroscopy. Sov. J. Quantum Electron. **17**, 168–173 (1987)
27. F.P. Schäfer: *Dye lasers* (Springer, Berlin, Heidelberg 1973) pp. 89, 93
28. V.M. Baev, K.-J. Boller, J. Eschner, A. Weiler, P.E. Toschek: Dynamics of a multimode dye laser after light injection. J. Opt. Soc. Am. B **7**, 2181–2186 (1990)
29. P. Goldberg, P.W. Milonni, B. Sundaram: Theory of the fundamental laser linewidth. Phys. Rev. A **44**, 1969–1985 (1991)